Electronic structure of 3d-transition-metal oxides: on-site Coulomb repulsion versus covalency

1999 J. Phys.: Condens. Matter 11 1657

(http://iopscience.iop.org/0953-8984/11/7/002)

J. Phys.: Condens. Matter **11** (1999) 1657–1682. Printed in the UK PII: S0953-8984(99)94380-1

Electronic structure of 3d-transition-metal oxides: on-site Coulomb repulsion versus covalency

R Zimmermann†, P Steiner†, R Claessen†§, F Reinert†, S Hüfner†, P Blaha‡ and P Dufek‡

† Fachrichtung Experimentalphysik, Universität des Saarlandes, D-66041 Saarbrücken, Germany
‡ Institut für Technische Elektrochemie, Technische Universität Wien, A-1060 Wien, Austria

Received 15 May 1998

Abstract. We have performed photoemission and inverse photoemission experiments on a series of 3d-transition-metal oxides with formal ionic configuration from $3d^0$ (TiO_2, V_2O_5) to $3d^{10}$ (Cu_2O). The photoemission core-level spectra are analysed in terms of a simple cluster model leading to estimates for the charge-transfer energy Δ, the Coulomb correlation energy U_{dd}, and the hybridization strength V. It is found that the ratio of the correlation energy to the hybridization energy significantly decreases from the late to the early transition metal oxides. This trend is attributed mostly to the increasing number of empty d states in the early transition metals which enhances the effective metal–ligand hybridization. We also compare the experimental valence band spectra with densities of states (DOS) from band-structure calculations. The rather good agreement between the theoretical DOS and the measured single-particle excitation spectra of the early 3d-transition-metal oxides as opposed to the failure of the one-electron description for most of the late transition metal oxides supports the results of the cluster model analysis.

1. Introduction

The oxides of the 3d transition metals (TM) show a rich variety of electronic properties, ranging from insulating to metallic or even superconducting behaviour. The same applies to their magnetic properties, where everything is found from Pauli paramagnetism to local moment behaviour including the occurrence of ferromagnetism and antiferromagnetism. Additionally, these materials can often be tuned from one electronic or magnetic phase to another by varying the temperature, pressure, or doping. Therefore, the TM oxides have for a long time been subjected to intensive experimental and theoretical study with the aim of finding a unifying description of their properties.

Historically, the first important step towards this goal was the formulation of the Mott–Hubbard (MH) theory [1–6], in which the electronic structure results from a competition between delocalization and localization of the 3d electrons. The former is described by the 3d-band width w, which is proportional to the frequency of hopping between neighbouring TM ions, whereas the Coulomb energy U_{dd} between 3d electrons on the same site stabilizes the ionic (i.e. local) character of the electronic structure. This model was devised to explain the insulating nature of NiO ($U_{dd} > w$), which in a one-electron picture would be metallic due to the partial occupation of the Ni 3d shell (formally d^8, Ni^{2+}). On the other hand, in its

§ New address: Experimentalphysik II, Universität Augsburg, D-86135 Augsburg, Germany.

0953-8984/99/071657+26$19.50

simplest form MH theory fails to account e.g. for the metallic behaviour of NiS, although here also $U_{dd} > w$. A comprehensive discussion of the properties of TM compounds within the framework of the MH picture is given in the reviews by Wilson [7–9]. They not only discuss the delicate balance between d–d hybridization and correlation, but also emphasize the subtle effects related to metal–anion (p–d) hybridization, coordination geometry, spin configuration, sub-band filling, and other aspects.

A new perspective on the problem was introduced by photoemission (PE) work in the early eighties. On the basis of the observation of satellites in TM core-level spectra, van der Laan *et al* [10] identified charge transfer (CT) from the ligand to the metal as another important electronic mechanism. In their model, main and satellite peaks were attributed to $|\mathrm{d}^{n+1}\underline{\mathrm{L}}\rangle$ ('well screened') and $|\mathrm{d}^{n}\rangle$ ('poorly screened') valence shell final states, where $\underline{\mathrm{L}}$ denotes a hole in the ligand shell and n is the number of 3d electrons in the ionic ground state. The interpretation of PE satellite structure as due to different screening channels was first proposed for La metal by Kotani and Toyozawa [11–13] on the basis of the Anderson impurity model [14], and subsequently applied to other metals and even insulators (the 'filled-band version') by Gunnarsson and Schönhammer [15, 16], Kotani *et al* [17], and Zaanen *et al* [18]. Neglecting the widths w and W of the TM 3d and ligand valence bands, respectively, one finally obtains the so-called cluster model which is equivalent to the above CT model [10], being based on a molecular orbital description [19–21]. This model describes the electronic structure of 3d-TM compounds in terms of three parameters: the CT energy Δ required to transfer an electron from a ligand valence orbital (in our case O 2p) to the TM 3d shell, the Coulomb interaction U_{dd} between two 3d electrons, and the hybridization V between the ligand and TM valence orbitals.

Zaanen, Sawatzky and Allen (ZSA) [22] proposed a scheme based on these parameters in which the TM compounds can be classified as CT ($\Delta < U_{dd}$) or MH systems ($U_{dd} < \Delta$), tacitly assuming that for most oxides the hybridization V plays only a minor role. First applications of this approach concerned compounds of the late 3d TMs and placed them in the CT regime of the ZSA diagram [23–26]. More recently, the picture was also applied to the excitation spectra of early TM compounds [27–30] which traditionally have been considered as typical MH systems [31–33]. However, it turned out that these materials are characterized by a strong effective hybridization $V^{eff} = \sqrt{n_h}V$ (n_h being the formal number of holes in the TM 3d orbital) which can no longer be neglected and, in fact, dominates their electronic structure, in contrast to a pure MH picture. The resulting covalency between TM 3d and ligand valence states (e.g. O 2p) promotes a delocalization of the TM 3d electrons, thereby reducing the importance of Coulomb correlation effects.

In this paper we present a systematic study of a series of TM oxides (TMO) by photoemission, inverse photoemission, cluster model, and band-structure calculations. The TMOs range from TiO_2 with a nominal d^0 configuration to Cu_2O with a formally closed 3d shell (d^{10}). The core-level spectra are analysed with the help of the cluster model to extract values for the parameters Δ, U_{dd}, and V (V^{eff}). Whereas this model approach emphasizes the localized aspects of the electronic structure, band calculations performed within density functional theory are able to account for lattice periodicity and delocalization of the valence electrons. On the other hand, they incorporate correlation effects only as far as they are relevant for the ground state, but not for the excited states probed by PE. The comparison of the calculated densities of states and the measured valence band spectra can therefore be regarded as an additional indicator for the importance of local correlations.

The organization of the paper is as follows. After giving a description of the experimental details in the following section, we sketch in section 3 the cluster model and the technical details of our band-structure calculations. Experimental spectra and their analysis in terms

of the two theoretical approaches are presented in sections 4 and 5. Section 6 contains a discussion of the results, which are finally summarized in section 7.

2. Experimental details

2.1. Photoemission and BIS

The XPS data have been measured with Al Kα radiation ($\hbar\omega = 1486.6$ eV) using three different spectrometers. Most of the data have been obtained on a Vacuum Generators (VG) ESCALAB MK2 spectrometer equipped with a twin anode for unmonochromatized Al/Mg Kα radiation and a monochromatized Al Kα source. The spectra for TiO_2, the vanadium oxides, Cr_2O_3, and the core levels of CrO_2 have been measured with a Surface Science Instruments 'M-Probe' spectrometer employing a monochromatized Al Kα source designed for small photon spots down to 150 μm. A Hewlett Packard HP 5950A spectrometer, also equipped with a monochromatized Al Kα source, served to collect the VB spectrum of CrO_2 and the Fe 2p/Fe 3p core-level spectra of Fe_2O_3. The resolution as determined from the width (FWHM) of the Au 4f lines was for all XPS measurements in the range 0.7–0.9 eV.

UPS measurements were performed using the VG spectrometer, using He I (21.2 eV) and He II (40.8 eV) radiation from a gas discharge lamp. The resolution of the UPS data amounts to about 0.1–0.2 eV. The raw UPS and unmonochromatized XPS data have been corrected for satellite radiation of the respective excitation lines.

Inverse photoemission experiments were performed in the bremsstrahlung isochromat spectroscopy (BIS) mode, using a tunable electron gun as the excitation source and the Al Kα x-ray monochromator of the VG spectrometer as a photon energy band-pass filter. The overall resolution amounts to 0.8 eV. Due to problems with sample size, sample charging, and electron-beam-induced surface decomposition—in the BIS mode, relatively high electron currents are required in order to obtain reasonable counting statistics—inverse photoemission data could only be taken for Cr_2O_3, MnO, Fe_2O_3, FeO, NiO, and Cu_2O.

All of the spectra were measured at room temperature, with the pressure typically in the low 10^{-10} mbar range.

2.2. Samples

The TiO_2 sample (rutile) was a commercially available pellet of polycrystalline material. For the vanadium oxides V_2O_5, VO_2, and V_2O_3, and the iron oxides FeO and Fe_2O_3, we used single crystals. The FeO crystal showed an Fe deficiency of about 5% ($Fe_{0.95}O$) [34] which leads to an effective hole doping of the sample, as reflected e.g. in the onset energy of the valence band spectrum (see section 5). The CrO_2 sample was also a polycrystalline pellet pressed from the powder. Cr_2O_3 was produced by *in situ* oxidation of a clean polycrystalline Cr metal foil as described elsewhere [35]. Similarly, polycrystalline CoO and NiO films have been created by oxidation of the corresponding metal substrates at about 550 °C and 10^{-5} mbar O_2 for about one hour and subsequent UHV annealing at 300 °C for several hours. MnO, Mn_2O_3, CuO, and Cu_2O were obtained by oxidizing the respective metal films deposited on a Pt substrate.

Clean sample surfaces, as characterized by the absence of a C 1s signal, have been obtained by different treatments. In the case of the thin films the metal substrates were first cleaned by smooth Ar etching and/or annealing (if necessary, in several cycles). Subsequent oxidation and—in some instances—an additional slight annealing resulted then in clean oxide films. For V_2O_5, clean surfaces were obtained by *in situ* cleavage of the single crystals, utilizing their layered structure [36]. All other sample surfaces were prepared by annealing to about 150 °C

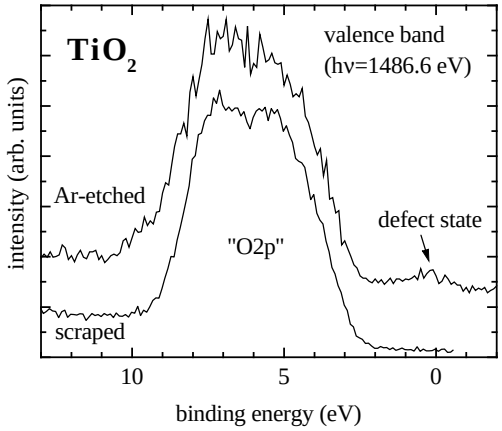

Figure 1. XPS valence band spectra of a freshly scraped and an Ar-sputtered surface of TiO_2. The defect states near the Fermi level created by the Ar bombardment indicate a reduction of the Ti ion upon oxygen depletion.

(to remove water) and subsequent scraping with a diamond file.

The problem of obtaining and also retaining monophase oxide surfaces especially in high-valence materials like TiO_2 (Ti^{4+}) and V_2O_5 (V^{5+}) is illustrated in figure 1. It shows, taking TiO_2 as an example, the formation of defect states on the low-binding-energy side of the O 2p band after Ar etching. This structure corresponds—in a very simplified picture—to an occupation of the Ti 3d valence shell in the formally $3d^0$ compound by creating O deficiencies during the sputtering procedure. Such defect states were also observed after heavy electron bombardment in BIS or after extended x-ray exposure (photon-induced surface defects). They are absent in a freshly scraped surface as shown in the lower spectrum. Where necessary, sample surfaces were repeatedly cleaned and measurements taken in short cycles, with good statistics obtained by accumulating the respective spectra.

Table 1. The optical gap E_{gap} for some 3d TMOs taken from the listed references. The numbers in parentheses are the gaps as determined from the combined PE/BIS spectra (see section 5). VO_2 and V_2O_3 undergo metal–insulator transitions at 340 K and 160 K, respectively. The band gaps E_{gap}^{bs} obtained from our band-structure calculations (see section 5) are also given for comparison. 'met.' denotes a metallic ground state.

TMO	E_{gap} (eV)	E_{gap}^{bs} (eV)	Reference
TiO_2	3.1	2.0	[74]
V_2O_5	2.0	2.0	[75]
VO_2	0.7/met.	met.	[76]
V_2O_3	0.2/met.	met.	[76]
CrO_2	met.	met.	[77]
Cr_2O_3	3.4 (3.2)	1.1	[78]
MnO	3.6–3.8 (3.9)	1.4	[79]
α-Fe_2O_3	2.0–2.7 (2.6)	0.55	[80]
FeO	2.4	0.25	[81]
CoO	2.4	0.5	[81]
NiO	4.0 (4.3)	1.0	[81]
CuO	1.4	—	[82]
Cu_2O	2.4 (2.3)	0.7	[82]

Finally, we note that, except for V_2O_3, which is metallic above 160 K [36], and for ferromagnetic CrO_2, which can be characterized as a semi-metal [37, 38], all oxides studied here are insulators at room temperature (cf. table 1). Some oxides (notably VO_2) showed inhomogeneous charging, which could be compensated by using a neutralizing flood gun during the photoemission measurements. An absolute energy scale was then established by shifting the valence band spectra in such a way as to place the Fermi level to the top of the insulator gap, simulating an effective n doping [39]. This procedure is not critical as we are mainly interested in *relative* energies. Charging did not occur in the thin-film oxides.

3. Theoretical methods

3.1. The cluster model

Here we give a brief overview on the cluster model (CM) approach used in this paper. A more detailed description of the method can be found in reference [39]. The idea is to describe the electronic structure and, in our particular case, the electron-removal spectra in terms of a few energy parameters: the ligand-to-metal charge-transfer (CT) energy $\Delta = E(\mathrm{d}^{n+1}\underline{\mathrm{L}}) - E(\mathrm{d}^n)$, the Coulomb correlation energy U_{dd} for two TM 3d electrons on the same atom, and the energy of hybridization ('rate of hopping') between TM 3d and O 2p orbitals. Here, n is the formal 3d occupation of the cation in a purely ionic picture, and $\underline{\mathrm{L}}$ denotes a hole in the O 2p shell. For core-level spectroscopy one has additionally to account for the Coulomb attraction U_{cd} between the PE core hole and a TM 3d electron, for which from atomic considerations [40] the relation $U_{dd} = \gamma U_{cd}$ with $\gamma \approx 0.7$–0.9 is assumed. The initial states and PE final states are expressed in terms of the configurations $|\mathrm{d}^{n+q}\underline{\mathrm{L}}^q\rangle$ and $|\underline{\mathrm{c}}\mathrm{d}^{n+q}\underline{\mathrm{L}}^q\rangle$, respectively, where $\underline{\mathrm{c}}$ denotes the PE core hole, and q gives the number of electrons transferred from the ligand orbital L to the TM 3d orbital. The effect of the metal–ligand hybridization is to mix the ionic eigenstates, yielding non-zero off-diagonal matrix elements of the cluster Hamiltonian (configuration interaction, CI). Information about the relevant model parameters can be derived from the PE core-level spectra by fitting the theoretical spectrum to the measured energy separation and spectral weight of the correlation satellites relative to the main line. With the help of these parameters one can then calculate the composition of the ground- and final-state wavefunctions and the corresponding 3d occupation numbers.

Different groups [41, 42] have extended the model to further include (besides CI) multiplet and crystal-field effects, allowing one to explain also the fine details of the spectral weight distribution. For example, multiplet splitting spreads the 3p spectra of 3d-TM compounds over an energy range of up to 20 eV, with the result that satellite structures are strongly affected by this interaction. In our calculation, we have neglected these effects and focused instead on a complete configurational basis set taking into account all ionic states $|\mathrm{d}^{n+q}\underline{\mathrm{L}}^q\rangle$ and $|\underline{\mathrm{c}}\mathrm{d}^{n+q}\underline{\mathrm{L}}^q\rangle$ with $q = 0, \ldots, 10 - n$. We will show that this becomes especially important for the case of strong covalency, as is relevant to the early TMOs.

For a given oxide we tried to reproduce all core-level spectra (usually TM 2s, 2p, 3s, and 3p) by using the *same* set of parameters Δ, U_{dd}, and V_i (the subscript i refers to the initial state), allowing only for a slight variation of the final-state parameters U_{cd} and V_f (final-state hybridization), which accounts for screening. This boundary condition will not in all cases lead to a perfect match of each individual experimental spectrum, because e.g. the core-level dependence of multiplet splittings neglected here will have to be absorbed by the parameters of our simplified model. Nonetheless, for all compounds studied here the overall agreement between measured and calculated model spectra is sufficient to allow the derivation of *trends* in the electronic structure from one oxide to the other.

CM calculations were performed for the oxides of Ti, V, Cr, and Fe. Here we restrict ourselves to the analysis of the core-level spectra, since valence band satellites are clearly observable only in the spectra of CrO_2 and Cr_2O_3 [43]. An inclusion of these valence bands in the cluster model analysis leads to parameter values consistent with those obtained from the core spectra, as shown elsewhere [43]. Finally, we wish to point out that for the early TMOs only few—if any—cluster model studies have been published so far.

3.2. Band-structure calculations

We also performed band-structure calculations using the full-potential linear augmented-plane-wave (LAPW) method as implemented in the WIEN97 code [44]. In this all-electron method, no shape approximations to potentials or charge densities are made, and scalar-relativistic equations neglecting spin–orbit interactions have been solved. All calculations are well converged in terms of the size of the plane-wave basis set and the k-point sampling within the irreducible part of the Brillouin zone. The density of states (DOS) was obtained using the improved tetrahedron method given by Blöchl *et al* [45]. In order to obtain partial densities of states (PDOS), the contributions of each state are weighted with the respective partial charge within the atomic sphere. Note, however, that within the LAPW scheme the decomposition of the total DOS into PDOS is not unique, but depends on the size of the atomic spheres. In addition, usually a sizable fraction of the charge is located outside the spheres and cannot be attributed to a particular atom. For example, using the same atomic sphere radii as in our band calculations, we find for free atoms between 3% (for Ni and Cu) and 35% (for V) of the d charge outside the integration volume.

The monoxides crystallize in the NaCl structure but were treated here in a rhombohedral cell including antiferromagnetism along the [111] direction [46,47]. The sesquioxides are also antiferromagnets and crystallize in the well known corundum structure, while the dioxides are non-magnetic insulators (TiO_2), non-magnetic metals (VO_2), or half-metallic ferromagnets (CrO_2) [37]. Finally, Cu_2O and V_2O_5 are non-magnetic insulators crystallizing in the cuprite and V_2O_5 structure, respectively. All structures refer to the respective room temperature phases.

Our band calculations are based on density functional theory (DFT) which applies strictly only to ground-state properties. It is well known that within the standard local spin-density approximation (LSDA) some of the late transition metal monoxides are metallic rather than being insulators [48]. For these reasons we have applied the generalized gradient approximation (GGA) to them, which in most cases is an improvement over LSDA, in particular for total energies and equilibrium properties [49]. The most common GGA, namely the one given by Perdew and Wang [50], was used for MnO and NiO, yielding insulators with sizable gaps (but still a factor of 2–4 too small) [47], while FeO and CoO are still metallic within this scheme. The problem was partly overcome by using the GGA parametrization given by Engel and Vosko [51], obtained by putting more weight on the exchange–correlation potential than on the respective energy. This yields also for FeO and CoO an insulating ground state [46,52], at least in qualitative agreement with experiment. However, it should be noted that equilibrium volumes are completely overestimated within this GGA [46].

4. Cluster model description of core-level spectra

Figures 2–9 show the experimental core-level XPS spectra for TiO_2, V_2O_5, VO_2, V_2O_3, CrO_2, Cr_2O_3, Fe_2O_3, and FeO, respectively, in comparison with the results of the cluster model calculations. Also included is the integrated background as suggested by Shirley [53] or, for

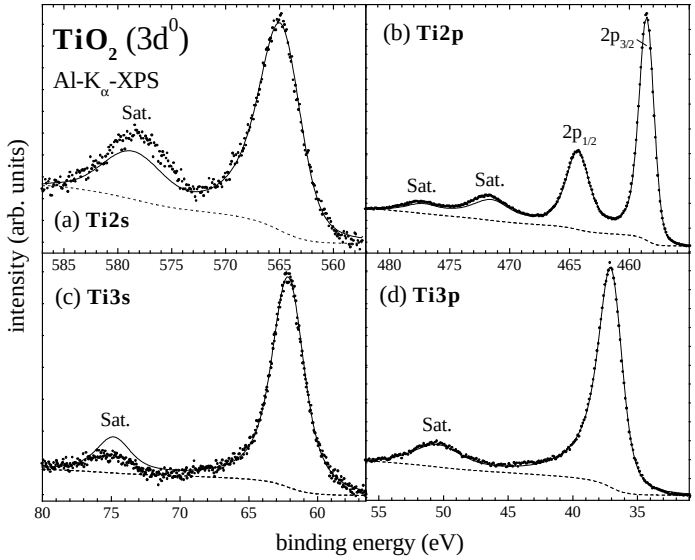

Figure 2. Experimental Ti 2s (a), Ti 2p (b), Ti 3s (c), and Ti 3p (d) core-level XPS spectra (dots) of TiO_2. Also shown are the calculated cluster model spectra (solid curves). The dashed curve in each panel indicates a Shirley-type background.

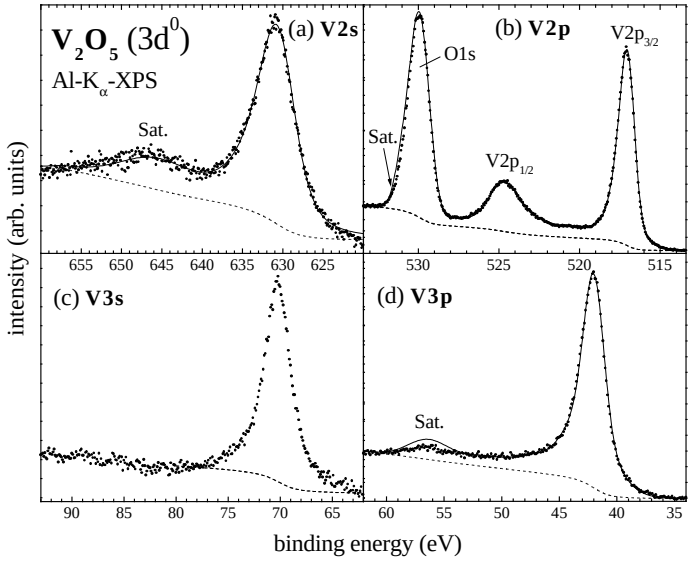

Figure 3. Experimental (dots) and calculated (solid curves) V 2s (a), V 2p (b), V 3s (c), and V 3p (d) core-level XPS spectra for V_2O_5. The 530 eV structure corresponds to the O 1s emission. The dashed curve in each panel indicates a Shirley background.

the iron oxides, a Tougaard background [54, 55] based on the electron energy-loss spectra (EELS) measured at 1000 eV primary energy [43, 56] with the electron gun also used to take the BIS data (cf. section 2).

We start the discussion of the experimental data with the TM 2s and 2p spectra. The former were only measured for TiO_2 and the vanadium oxides, and are dominated by substantial

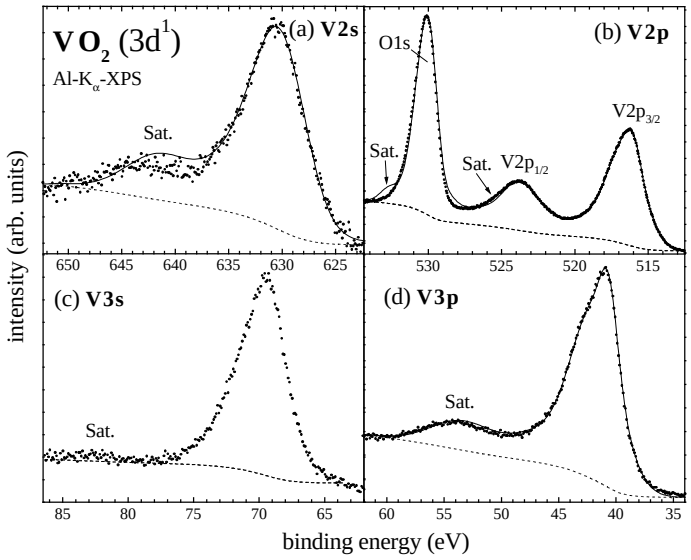

Figure 4. As figure 3, but for VO_2.

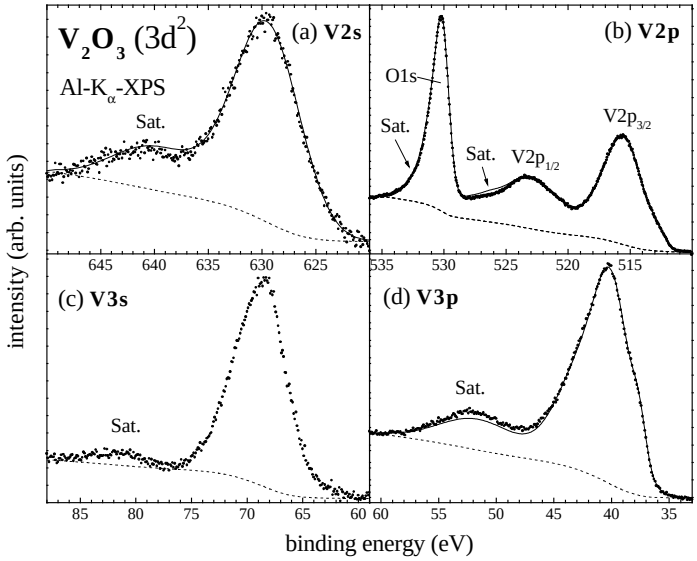

Figure 5. As figure 3, but for V_2O_3.

lifetime broadening due to the rapid decay of the excited core-hole state. Nonetheless, in all cases a clearly visible satellite structure accompanies the main line feature. The 2p spectra are characterized by strong spin–orbit splitting into $2p_{1/2}$ and $2p_{3/2}$ parts, and this increases with the atomic number of the TM from TiO_2 (less than 6 eV), through the vanadium oxides (7–8 eV) and the chromium oxides (nearly 10 eV), to a value of more than 12 eV for the iron oxides. Whereas in TiO_2 the satellites are well separated from the corresponding main lines, they interfere strongly in the vanadium oxides with the $2p_{1/2}$ peak and the O 1s line at 530 eV, which complicates a quantitative analysis [39]. In CrO_2 and Cr_2O_3, at least the $2p_{1/2}$

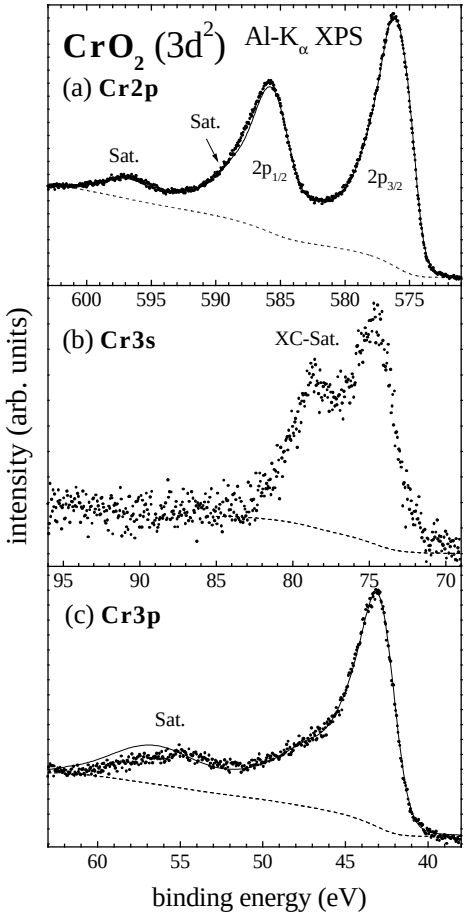

Figure 6. Experimental (dots) and calculated cluster model (solid curves) core-level spectra for CrO_2.

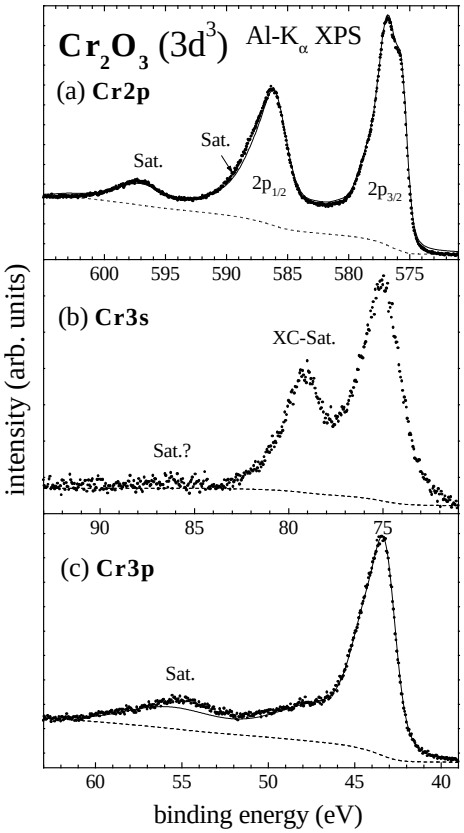

Figure 7. Experimental (dots) and calculated cluster model (solid curves) core-level spectra for Cr_2O_3.

satellite is clearly separated from the main peak. In the iron oxides, the interference of main and satellite lines is again very strong and further complicated by the occurrence of a second satellite. The origin of the feature at 744 eV in the Fe 2p spectrum of FeO (figure 9) is not clear at the moment. Its separation from the main line ($\approx$20 eV) seems too large for an interpretation as a second CT satellite of the $2p_{1/2}$ peak, since this value is much larger than the separation of the second satellite in Fe_2O_3. The structure could possibly be due to an inelastic plasmon excitation, as its relative position coincides with that of a loss structure observed in the O 1s and EELS spectra [43].

The TM 3s spectra are governed by exchange coupling of the spin of the 3s core hole to the total spin S of the 3d valence shell [57, 58]. In atomic theory [59] this causes a splitting proportional to S, with the intensity ratio between the split peaks given by $S/(S+1)$. For late TM compounds this picture seems to work reasonably well, allowing one to use the splitting as a rough measure for the 3d occupation [60, 61]. In contrast, for intermediate-to-early TM compounds there seems to be no clear correlation of the exchange splitting with the actual d occupation or the magnetic moment [39, 62]. On the other hand, the splitting does show a tendency to increase with the *formal* d occupation [63]. Accordingly, no exchange splitting

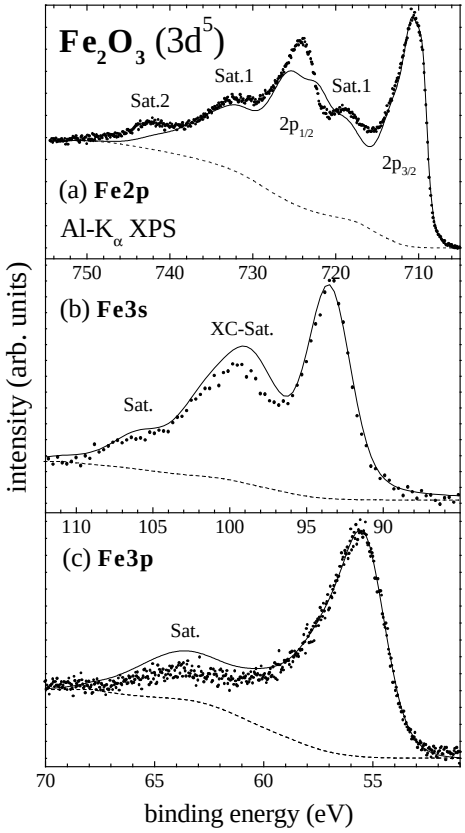

Figure 8. Experimental (dots) and calculated cluster model (solid curves) core-level spectra for Fe_2O_3. The dashed curve in each panel indicates a Tougaard background.

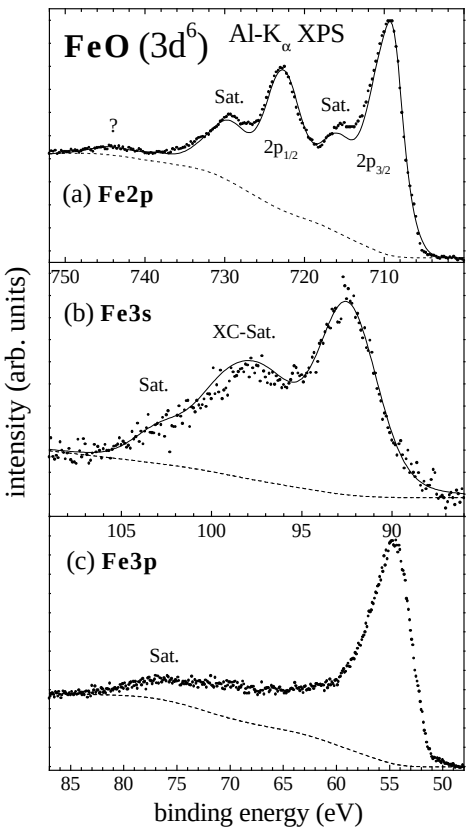

Figure 9. Experimental (dots) and calculated cluster model (solid curves) core-level spectra for FeO. The dashed curve in each panel indicates a Tougaard background.

is observed in the d^0 compounds TiO_2 and V_2O_5. The main 3s line shows an increasing broadening from VO_2 to V_2O_3 to CrO_2, and a well separated exchange satellite ('XC-Sat.') split off by 4.1 eV is observed in the d^3 compound Cr_2O_3. In the iron oxides the exchange splitting and CT satellite contributions strongly interfere [60,61], making a quantitative analysis rather difficult. Therefore, the corresponding values for ΔE_{sat}^{exp} and $(I_{sat}/I_m)^{exp}$ in table 3—see later—have to be treated with some caution. Compared to the case for the other core spectra, the correlation satellites in the 3s spectra were found to be of very low intensity for all materials studied. In fact, they were clearly observable only for TiO_2, VO_2, V_2O_3, and the iron oxides. This behaviour is presumably related to CI between the PE final states $3s^1 3p^6 3d^n$ and $3s^2 3p^4 3d^{n+1}$ [64, 65], which is not contained in our simple cluster model.

The TM 3p spectra also exhibit a satellite structure quite well separated from the main line. Contrary to the case for the 2p spectra, the spin–orbit splitting is small and is only reflected in a broadening of the main lines (again increasing from TiO_2 to the iron oxides). However, for some compounds, pronounced multiplet splitting makes a precise determination of satellite position and weight very difficult. The effect is particularly strong in FeO (figure 9), where the satellite structure in the 3p spectrum extends over more than 10 eV, making a cluster model analysis without the inclusion of multiplets more or less meaningless. The multiplet splitting

originates from the coupling between the photoexcited core-level configuration and the partly filled TM 3d shell. Since the spatial extension of 3p and 3d states is similar, multiplet effects are strong in the 3p spectra. In contrast, in the TM 2p spectra the multiplet interaction leads only to a slight broadening of the PE peaks, because the 2p states reside much closer to the ion core than the 3d valence electrons.

Before proceeding to the CM analysis, we have to check whether the observed satellites arise exclusively from (intrinsic) final-state effects, or whether extrinsic losses, e.g. due to plasmon excitation, contribute to them, especially in those cases where the main line-to-satellite separation takes a value of a typical plasmon energy (10–20 eV). This was done by comparing the TM core-level data to the corresponding O 1s spectra, which would contain extrinsic plasmon satellites, if they exist, but not 3d correlation-related features (at least not to the same extent as observed in the TM spectra). For some compounds we determined the loss spectrum directly by EELS in order to perform a Tougaard background correction [54] (see e.g. the Fe spectra in figures 8 and 9). Both methods clearly confirm that the satellites discussed above are of intrinsic nature [43]. This conclusion is also supported by the fact that the satellite intensity in the 3s core-level spectra is in all cases much lower than for the other core levels, which should not be the case if they originate from extrinsic plasmon losses.

Table 2. Cluster model parameters Δ, U_{dd}, and V_i for the oxides analysed in this paper. Also listed are parameters for CoO, NiO, and CuO obtained by the same method, but published elsewhere. The last three columns contain the effective initial-state hybridization $V_i^{eff} = \sqrt{n_h} V_i$, the formal number n_h of 3d holes, and the ratio U_{dd}/V_i^{eff}, respectively. All energies are in eV.

	Δ	U_{dd}	V_i	V_i^{eff}	n_h	U_{dd}/V_i^{eff}
TiO_2	4.0	5.0	2.8	8.9	10	0.56
V_2O_5	3.5	4.5	3.6	11.4	10	0.40
VO_2	4.4	3.8	2.5	7.5	9	0.51
V_2O_3	5.5	3.8	2.3	6.5	8	0.58
CrO_2	5.5	5.5	2.8	7.9	8	0.69
Cr_2O_3	6.0	5.5	2.8	7.4	7	0.74
Fe_2O_3	5.5	5.5	1.8	4.0	5	1.37
FeO	6.3	5.3	1.8	3.6	4	1.46
CoO[a]	6.0	4.7	1.6	2.8	3	1.67
NiO[a]	4.5	5.9	2.7	3.8	2	1.55
CuO[b]	3.2	6.5	3.0	3.0	1	2.17

[a] From reference [31].
[b] From reference [83].

As a prerequisite for the CM analysis, we determined the relative energy positions ΔE_{sat}^{exp} and spectral intensities $(I_{sat}/I_m)^{exp}$ of the main and satellite peaks by least-squares fits of the spectra, using a combination of Lorentzian and Gaussian line profiles (not shown here). The neglect of more realistic lineshapes related to, e.g., electron–hole pair shake-up (as in metallic V_2O_3) or low-energy plasmon satellites resulting from narrow d bands is of marginal importance for our CM analysis, with the possible error clearly smaller than the uncertainty in the inelastic background subtraction. CM calculations were then performed so as to give the best coincidence between experiment and theory for all core levels of a given compound, as described above (cf. section 3.1). The resulting model parameters Δ, U_{dd}, and V_i as well as the effective initial-state hybridization $V_i^{eff} = \sqrt{n_h} V_i$, with n_h being the formal number of 3d holes on the cation, are listed in table 2. In addition, table 3 gives the final-state parameters U_{cd}, V_f, and V_f^{eff}, and the calculated 3d occupation numbers of the ground state (n_d^{cm}) and the final states corresponding to main (n_m^{cm}) and satellite (n_{sat}^{cm}) lines. This table also

Table 3. Cluster model parameters U_{cd}, V_f, and the effective final-state hybridization $V_f^{eff} = \sqrt{n_h}V_f$ for 2s, 2p, 3s, and 3p core-level photoemission. The resulting occupation numbers for the ground state (n_d^{cm}) and photoemission final states (main line n_m^{cm}, satellites n_{sat}^{cm}) are shown together with the formal values n_d. Also listed are the relative satellite separations and intensities obtained from the cluster model (ΔE_{sat}^{cm}, $(I_{sat}/I_m)^{cm}$) in comparison with the respective experimental values (ΔE_{sat}^{exp}, $(I_{sat}/I_m)^{exp}$). The two rows for the Fe 2p spectra correspond to the first and second satellites, respectively. All energies are in eV.

		V_f	V_f^{eff}	U_{cd}	n_d	n_d^{cm}	n_m^{cm}	n_{sat}^{cm}	ΔE_{sat}^{cm}	ΔE_{sat}^{exp}	$(I_{sat}/I_m)^{cm}$	$(I_{sat}/I_m)^{exp}$
TiO_2	2s	3.2	10.0	6.2	0	1.0	1.8	1.8	13.0	12.6	0.25	0.35
	2p	3.2	10.0	6.1			1.8	1.8	13.0	13.2[a]	0.24	0.28[a]
	3s	3.1	9.6	5.5			1.7	1.7	12.7	13.2	0.19	0.10
	3p	3.1	9.6	5.7			1.7	1.7	12.7	12.6	0.20	0.21
V_2O_5	2s	3.9	12.3	5.9	0	1.3	2.1	2.1	14.7	15.0	0.19	0.20
	2p	3.6	11.4	5.3			2.0	2.0	13.9	14.1[b]	0.13	0.06[b]
	3p	3.6	11.4	5.0			1.9	1.9	13.9	13.9	0.12	0.07
VO_2	2s	2.6	7.8	4.5	1	1.9	2.5	2.6	10.1	11.6	0.16	0.12
	2p	2.5	7.5	4.4			2.5	2.5	9.8	9.3[a]	0.14	0.11[a]
	3p	2.9	8.7	4.2			2.6	2.6	11.0	11.3	0.18	0.16
V_2O_3	2s	2.8	7.9	4.5	2	2.6	3.3	3.4	10.3	10.7	0.21	0.19
	2p	2.8	7.9	4.5			3.3	3.4	10.3	10.5[a]	0.21	0.18[a]
	3p	2.9	8.2	4.3			3.3	3.4	10.6	10.5	0.21	0.25
CrO_2	2p	2.8	7.9	6.8	2	2.7	3.4	3.4	11.4	11.2[a]	0.22	0.24[a]
	3p	2.8	7.9	6.1			3.3	3.3	11.3	10.0	0.18	0.13
Cr_2O_3	2p	3.1	8.2	6.7	3	3.6	4.3	4.3	11.7	11.7[a]	0.25	0.32[a]
	3p	2.8	7.4	6.2			4.2	4.2	10.8	10.3	0.18	0.24
Fe_2O_3	2p	1.9	4.3	8.0	5	5.3	6.2	6.2	7.4	7.1[a]	0.59	0.65[a]
								6.1	12.7	14.2[a]	0.12	0.19[a]
	3s	2.1	4.7	6.1			6.0	5.9	7.8	7.8[c]	0.35	0.28[c]
	3p	1.8	4.0	6.1			6.0	5.9	6.9	6.9	0.31	0.18
FeO	2p	1.8	3.6	7.5	6	6.2	7.0	6.9	6.4	6.1[a]	0.52	0.56[a]
								7.3	11.0	11.4[d]	0.05	0.08[d]
	3s	1.9	3.8	5.8			6.8	6.8	6.5	6.7[c]	0.27	0.23[c]

[a] Mean values from $2p_{3/2}$ and $2p_{1/2}$ satellites.
[b] Only from the $2p_{3/2}$ satellite.
[c] Mean values from exchange-split 3s lines.
[d] Only from the $2p_{1/2}$ satellite.

contains the calculated satellite intensities and separations from the main line in comparison to the experimental values, which gives some indication of the quality of the individual fits. The theoretical spectra (shown as solid curves in figures 2–9) have been constructed from the calculated satellite positions and intensities and the linewidths obtained in the least-squares fits.

From the comparison of the theoretical and experimental results in figures 2–9 and table 3, one finds that our cluster model is—despite its simplicity—able to reproduce the measured data quite well. In a few instances deviations occur between measured and calculated results, which can be attributed to the neglect of more complicated CI and multiplet effects. This concerns e.g. the 3s-satellite intensities, as already discussed above; only for TiO_2, Fe_2O_3, and FeO we were able to reproduce the experimental 3s spectra with reasonable model parameters. There is also a problem with the 2p satellites in VO_2, which may reflect the difficulty of finding an

unambiguous spectral decomposition due to the strong overlap of main line, satellite, and O 1s intensities. The poor CM approximation of the 2p spectrum of Fe_2O_3 will be commented on in section 6. Apart from that, the least-squares-fit analysis of the experimental spectra yields consistent values of ΔE_{sat} and I_{sat}/I_m for all core levels of a given oxide. Consequently, the CM parameters obtained from them can be viewed as fairly reliable estimates. They show interesting behaviour and trends across the TM oxide series, which in the following will be discussed in more detail.

As seen from table 2, the charge-transfer energy Δ and the 3d-electron interaction U_{dd} show a slight and non-systematic variation over the energy range 4–6 eV. The apparent scatter of these parameters reflects the fact that the theoretical spectra are relatively insensitive to their absolute values. Rather, it is the *difference* $\Delta - U_{cd}$ (with U_{cd} being close to U_{dd} as discussed in section 3.1) which affects the separation and intensity of the first satellite (only one satellite is observable for the early TMOs). The CM calculations are much more sensitive to the hybridization energies V_i and V_f: slight variations by only a few tenths of an eV cause large changes in the theoretical spectra. Therefore, the decrease of the hybridization by 1.0–1.5 eV from the early TMOs to CoO can be taken as statistically significant. The large hybridization parameter values for V_2O_5 relative to those of the other vanadium oxides are attributed to the lower average vanadium–oxygen distance in this compound [36]. An increased hybridization strength is also found again for NiO and CuO. For CuO this may likewise be related to a relatively small TM–O bond length (1.98 Å compared to 2.13 and 2.16 Å in the other monoxides CoO and FeO, respectively). For NiO ($d_{\mathrm{TM-O}} = 2.08$ Å) this is less clear. The hybridization V_f in the photoemission final state was for all oxides found to be equal to or only slightly larger than that in the ground state (V_i).

In order to fully appreciate the role of metal–ligand covalency, one should look not at the bare hybridization energy V, but rather at the *effective* hybridization strength $V^{eff} = \sqrt{n_h}V$, which in our CM Hamiltonian is the matrix element connecting the formally ionic ground state $|\mathrm{d}^n\rangle$ and the first charge-transfer state $|\mathrm{d}^{n+1}\underline{\mathrm{L}}\rangle$, with $n_h = 10 - n$. It is a far better measure for covalency effects, because it takes full account of the phase space available for charge transfer from the ligand onto the 3d shell. Looking at the corresponding values V_i^{eff} and V_f^{eff}, one finds that the effective hybridization is the dominating energy term for the early TMOs, up to a factor of 3 larger than the other parameters. Going towards the heavier TMs, its magnitude decreases systematically and becomes comparable to or even smaller than Δ and U_{dd} for the iron oxides and beyond. With the bare hybridization displaying only little variation, this trend results mostly from the decreasing number n_h of holes in the TM 3d shell.

The varying influence of covalency on the electronic structure is demonstrated in figure 10, which contains the energy level diagrams for TiO_2 and FeO as examples for an early and an intermediate-to-late TMO, respectively. The figure shows the energies of the first three eigenstates calculated without ($V = 0$) and with ($V > 0$) hybridization using the initial-state (N-electron) and final-state (($N-1$)-electron) cluster model Hamiltonians. In TiO_2 the strong hybridization pushes the ionic configurations far apart and leads to an energy gain of the N-electron ground state by as much as $\approx$11 eV (nearly 20 eV in the lowest core-hole state). In contrast, the effect is much reduced in FeO, where the corresponding hybridization gain is only $\approx$2 eV.

The destabilization of the ionic state in the early TMOs can also be seen from the decomposition of the ground and 2p PE final states into the basis states $|\mathrm{d}^{n+q}\underline{\mathrm{L}}^q\rangle$ and $|\underline{\mathrm{c}}\mathrm{d}^{n+q}\underline{\mathrm{L}}^q\rangle$, respectively, shown in figure 11. Non-negligible contributions of states with q-values up to 3 in the ground state and even up to 5 in the core-hole states indicate a pronounced delocalization of the TM 3d electrons upon hybridization. In TiO_2 and V_2O_5 the contribution of the formal ionic state is not even close to that with the highest fractional parentage. For the ground

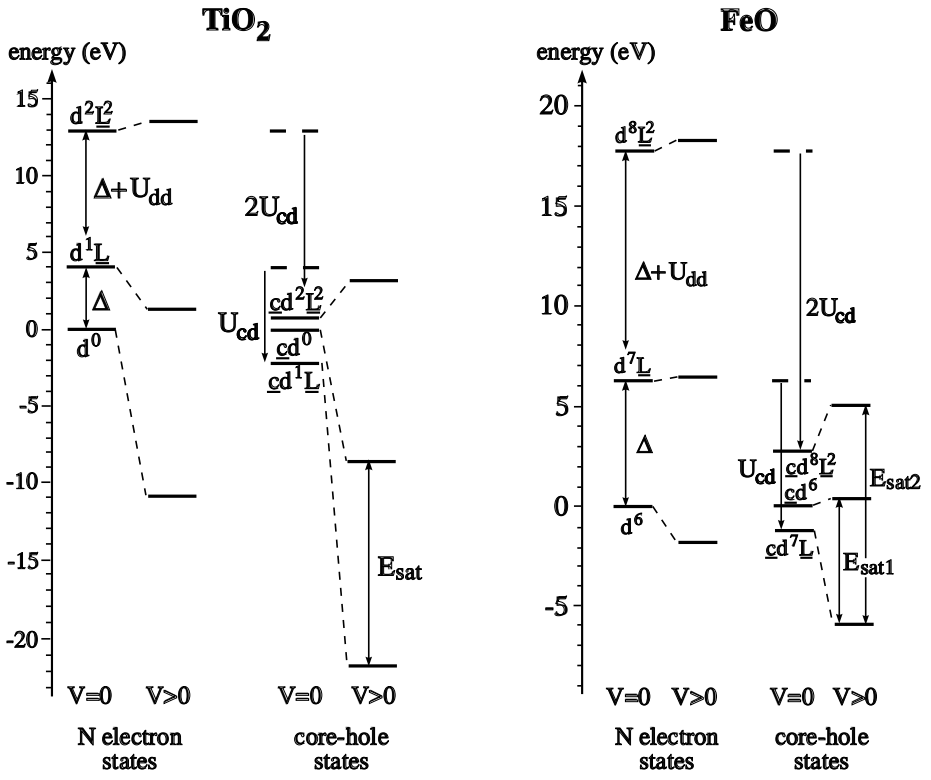

Figure 10. Energy level diagrams for TiO_2 and FeO obtained from the cluster model calculations. The diagrams show the lowest three eigenstates of the neutral (N-electron states) and photoexcited (core-hole states) systems in the purely ionic limit ($V = 0$) and in the presence of TM 3d–O 2p hybridization ($V > 0$). Note the dramatic effects of covalency in TiO_2.

states of the iron oxides one finds in contrast that they are clearly dominated by the ionic $|\mathrm{d}^n\rangle$ configuration. The situation is somewhat different for the PE final states, because here the combined effects of Δ, U_{dd}, and the core-hole potential U_{cd} pull the unhybridized states close together (cf. figure 10). As a consequence their energy separation becomes small compared to V_f^{eff}, so there is then an enhancement of the mixing of ionic configurations, as seen in figure 11. For the late TMOs NiO and CuO, nearly ionic behaviour is stabilized also in the final state (not shown here).

As a consequence of the pronounced hybridization in the early TMOs, the average 3d ground-state occupation number n_d^{cm} obtained in the CM analysis is considerably larger than the value n_d expected from a purely ionic picture (table 3). This is particularly evident for the formally d^0 materials TiO_2 and V_2O_5, where the 3d shell contains on average at least one electron. In contrast, for the iron oxides, n_d^{cm} is found to be fairly close to the ionic limit. As regards the occupation numbers n_m^{cm} and n_{sat}^{cm} for the PE final states (main line and satellite, respectively), we find that the core-hole potential lowers the energy of the 3d shell in such a way as to accommodate approximately one electron more than in the ground state. Due to the strong CI in the early TMOs, n_m^{cm} and n_{sat}^{cm} are very similar. This is still true for the iron oxides, although here mixing between basis states clearly diminishes and one basis state starts to dominate at least the main-line final state ($|\underline{c}\mathrm{d}^6\underline{\mathrm{L}}\rangle$ for Fe_2O_3 and $|\underline{c}\mathrm{d}^7\underline{\mathrm{L}}\rangle$ for FeO). While it is well established that the PE final states in the late TMOs like NiO or CuO can be labelled by

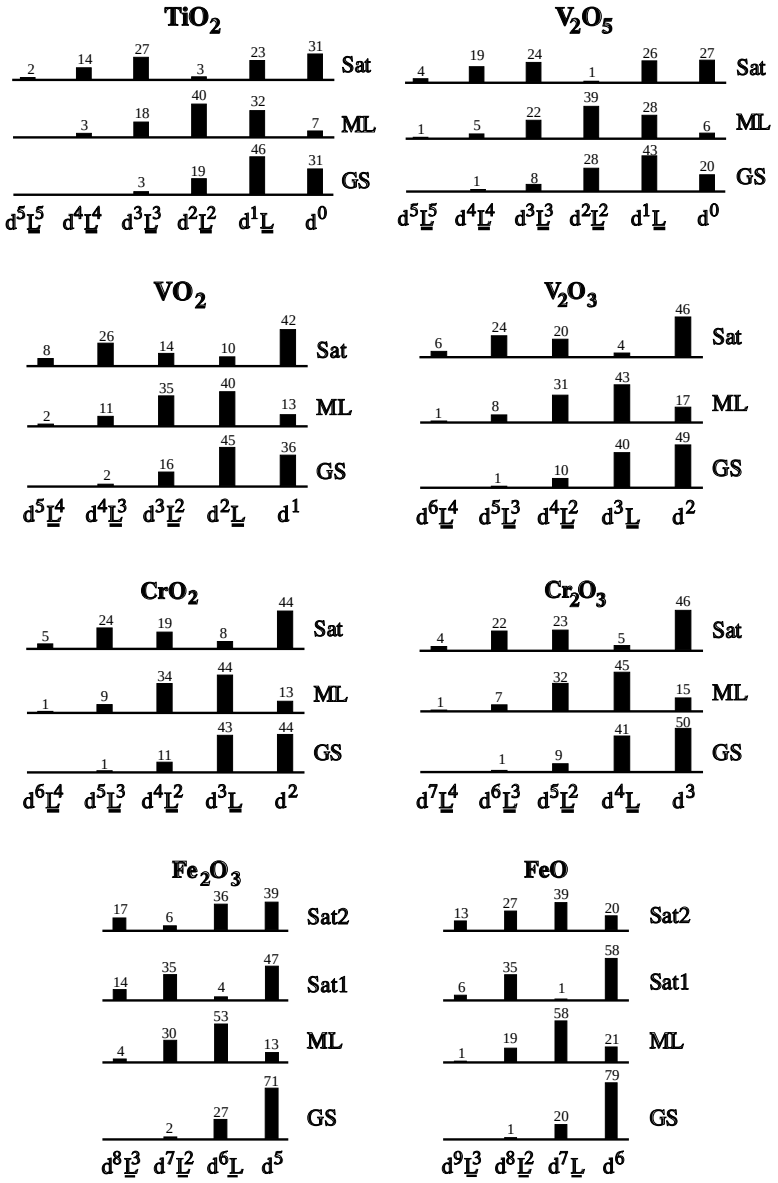

Figure 11. The fractional parentage of the various basis states in the N-electron ground state (GS) $|\psi_g\rangle$ and the PE final states $|\psi_m\rangle$ (ML = main line) and $|\psi_{sat}\rangle$ (Sat = satellite), obtained from the cluster model for the case of TM 2p PE. The numbers labelling the bars denote the percentages of the respective fractional occupations.

a single ionic configuration $|\underline{c}d^{n+q}\underline{L}^q\rangle$ [31], our results show that this is no longer meaningful for the strongly covalent early TMOs, with the iron oxides providing the borderline.

As regards a comparison of our cluster model results to those of other studies, we wish to point out that the meaning of the various model parameters can vary according to the inclusion of multiplet, crystal-field, and/or spin–orbit effects, and the use of a more restricted basis set than in our work. Therefore, absolute numbers may deviate slightly between the various

models and are not easily mapped onto each other. Nonetheless, the global trends across the 3d TM series found in this and other studies are largely consistent. Values for TiO_2 [29, 65], V_2O_5 [29], VO_2 [28], V_2O_3 [29, 30], Cr_2O_3 [30, 32], Fe_2O_3 [30], and FeO [24, 66] can be found in the literature.

5. Valence band spectra and band-structure calculations

We now focus our attention on the valence and conduction band states. Unlike the core levels, these states tend to delocalize due to nearest-neighbour hopping. It is clear that the cluster model, being based on a localized picture, cannot account for the formation of *bands*. Alternatively, one can calculate the valence and conduction band structure within density functional theory (DFT). Here, the interaction of the electrons with the periodic crystal potential is fully included and leads to itinerant Bloch states. The Coulomb interaction between the electrons is treated in a self-consistent way, such that electronic correlations in the ground state are correctly accounted for (at least approximately, as in the case of the LSDA). The shortcoming of DFT calculations is however that they do not contain the correlation effects (e.g., satellite structures) relevant for excitations from the ground state. As a consequence, the agreement or disagreement between the calculated density of states (DOS) and the experimental PE and BIS spectra yields information on the effect of correlations on the single-particle spectra ('self-energy effects'). In the following we will therefore compare the experimental valence band photoemission (XPS, UPS) and inverse photoemission (BIS) spectra of a series of 3d TMOs with the corresponding DFT band-structure calculations.

Figures 12 and 13 give an overview of the total and partial O 2p and TM 3d DOS calculated for TiO_2, V_2O_5, VO_2, V_2O_3, CrO_2, Cr_2O_3, MnO, Fe_2O_3, FeO, CoO, NiO, and Cu_2O. For all oxides one can distinguish two regions separated by a more or less pronounced gap: a broad band of predominantly O 2p character at low energies, and a somewhat sharper TM 3d-like band at higher energies. The sharp structures or even gaps (for the late TMOs) in the TM 3d bands can be attributed to crystal-field splitting of the 3d states in the (distorted) octahedral ligand environment 'seen' by the TM ions in most of these oxides. Going from the early to the late TMOs, i.e. with increasing formal d occupation, the Fermi level shifts into the TM 3d band.

The resulting gaps between occupied and unoccupied DOS are generally too small compared to those measured by optical spectroscopy or combined PES/BIS (see table 1). This is related to the already discussed failure of DFT to describe excitations correctly (cf. section 3.2). For V_2O_3 the LSDA result shown in figure 12 even yields a metallic state, although the calculation was performed for the insulating antiferromagnetic phase. Using the GGA instead results in a strong quenching of the DOS at the Fermi level, but still leaves the ground state metallic (not shown here) and shows worse correspondence with the experimental spectra than the LSDA. For VO_2 we have to add that the calculation has been performed for the undistorted metallic phase.

Hybridization between ligand and metal states can be seen from the fact that there is a non-negligible TM 3d partial DOS (PDOS) in the range of the 'O 2p' band and vice versa. In the case of the d^0 compounds TiO_2 and V_2O_5, this leads to a finite d occupation, in accordance with the CM result of the previous section. At the other end of the TM series, Cu_2O with a formally fully occupied 3d shell shows a non-zero Cu 3d PDOS in the unoccupied energy region, which should be detectable by BIS.

The d occupation numbers n_d^{bs} derived from the band calculations are listed in table 4 in comparison to those obtained in the CM analysis (n_d^{cm}) and the purely ionic limit (n_d). The two theoretical methods yield largely consistent values. An interesting difference is however

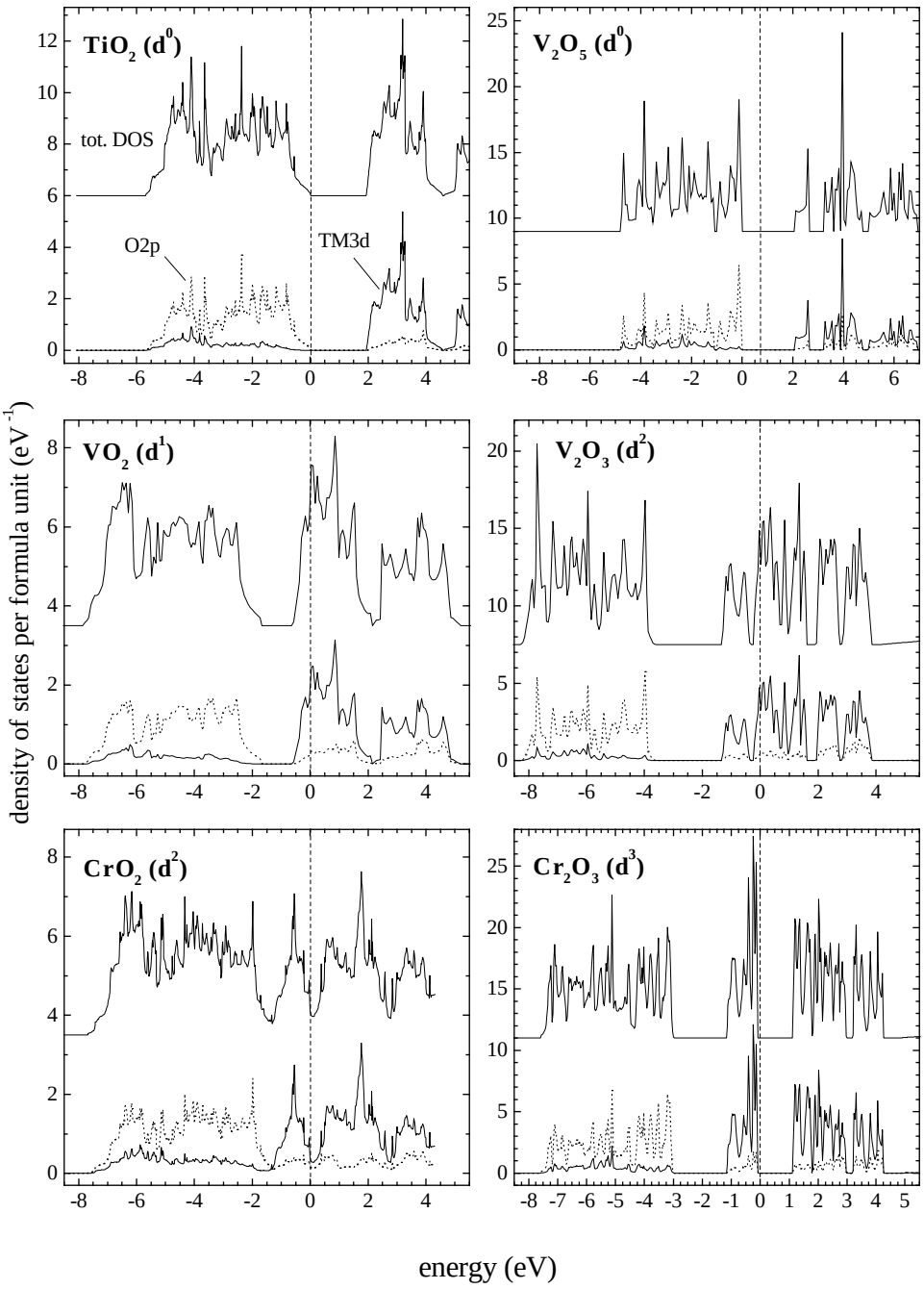

Figure 12. Total (upper solid curves) and partial TM 3d (lower solid curves) and O 2p (dotted curves) densities of states (DOS) obtained by density functional band-structure calculations for the early TM oxides TiO_2, V_2O_5, VO_2, V_2O_3, CrO_2, and Cr_2O_3. The total DOS is offset for improved clarity. Both total and partial DOS are normalized to the formula unit of each oxide. Energies are given relative to the Fermi energy, which in the case of the insulators was arbitrarily placed at the top of the valence band.

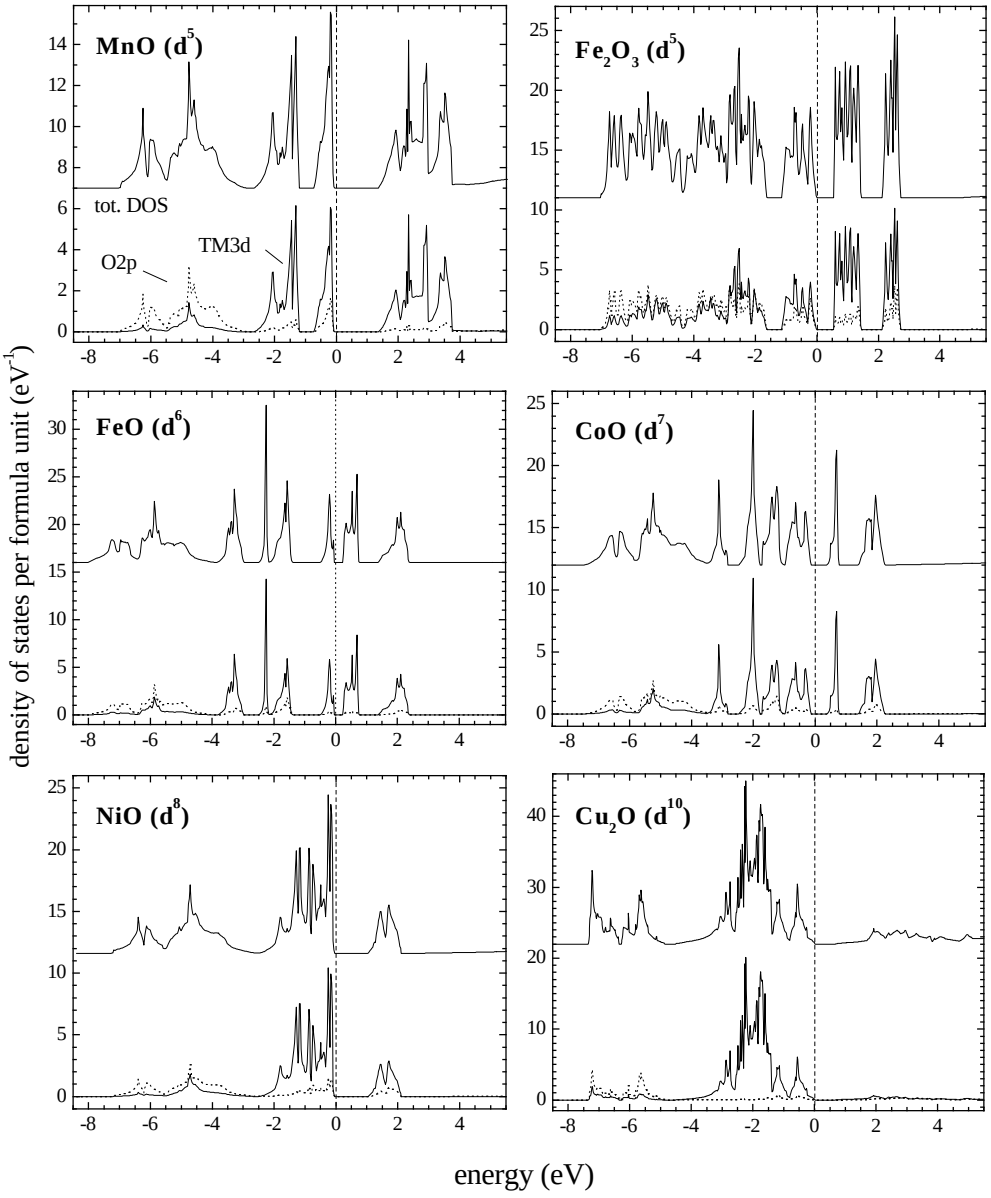

Figure 13. As figure 12, but for the late TM oxides MnO, Fe_2O_3, FeO, CoO, NiO, and Cu_2O.

observed when comparing the numbers for the various oxides of the same TM (V, Cr, and Fe in table 4): the band theoretical d occupation depends only on the particular TM and displays very little dependence on its formal valence ($\Delta n_d^{bs} = 0.1$–0.2 electrons per valence step), in contrast to the CM results. A similar lack of correlation of the calculated n_d^{bs} with the chemical valence has been reported for the oxides of Cu [67–69]. Although there is a certain degree of freedom in choosing the appropriate atomic sphere radius r_{as} (cf. table 4), over which the partial d charge is integrated in order to obtain n_d^{bs}, it does not explain the contradictory trends of the band theory and the cluster model. In principle, the DFT should yield the exact ground-state 3d

Table 4. Transition metal 3d occupation numbers for the ionic limit (n_d), obtained from the cluster model analysis of the PE core spectra (n_d^{cm}), and derived from the band-structure calculations (n_d^{bs}). r_{as} denotes the atomic sphere radius used to determine the d charge in the band calculation.

	n_d	n_d^{cm}	n_d^{bs}	r_{as} (Å)
TiO_2	0	1.0	1.3	1.06
V_2O_5	0	1.3	1.7	0.79
VO_2	1	1.9	1.7	0.79
V_2O_3	2	2.6	1.9	0.79
CrO_2	2	2.7	3.1	0.95
Cr_2O_3	3	3.6	3.3	0.95
MnO	5	5.1[a]	4.7	1.06
Fe_2O_3	5	5.3	5.2	0.95
FeO	6	6.2	5.5	0.95
CoO	7	7.2[a]	6.8	1.06
NiO	8	8.3[a]	7.9	1.06
Cu_2O	10	—	8.8	1.01

[a] From reference [43].

occupation. However, one may speculate that the L(S)DA used for the exchange–correlation potential in the band calculations underestimates the effect of the local Coulomb repulsion which stabilizes the valence. On the other hand, our simplified cluster model neglects non-local effects going beyond a single TM ion and its immediate ligand shell (e.g. 'non-local screening' [70, 71]), and may therefore overemphasize the importance of ionic valency. In this case the number n_d^{cm} derived in a CM analysis should not be taken as reflecting the actual 3d-electron count at the TM site, but rather as some 'effective' charge which is characteristic of the particular TM valence. In view of these considerations, the *overall* agreement between the cluster model and band theory occupation numbers is remarkably good.

It is interesting to study the spectral distribution of the 3d weight obtained in the band calculations in more detail, taking the vanadium oxides as an example. Here the occupied part of the 'TM 3d'-like band complex close to the Fermi level (cf. figure 12) is found to contain 0, 0.6, and 1.2 V 3d electrons in V_2O_5, VO_2, and V_2O_3, respectively, which scales with but is significantly smaller than the formal d count (0, 1, and 2, respectively). On the other hand and as already noted above, the *total* V 3d charge in the respective atomic spheres shows only little variation (table 4). This is explained by the fact that at the same time the V 3d contribution in the predominantly O 2p bands at higher binding energy is reduced (1.6, 1.1, 0.7 V 3d electrons in this series), leaving the total V 3d occupancy nearly unchanged. Thus, V_2O_5 can be considered to be much more covalently bonded than V_2O_3, with VO_2 lying between them. This result is in agreement with the CM analysis (table 2).

We have measured the XPS valence band spectra for all oxides contained in figures 12 and 13. Where charging did not prevent it, we also took valence band spectra with He I and He II (not shown here) radiation and measured the unoccupied states additionally by BIS. Figures 14 and 15 show the experimental data together with the theoretical results. In order to facilitate a better comparison between theory and experiment, the calculated densities of states have been convoluted with a Gaussian line profile, which was done to simulate the effects of both finite instrumental resolution and lifetime broadening of the excited states. The full width at half-maximum (FWHM) of the Gaussian was chosen to roughly reproduce the widths of the

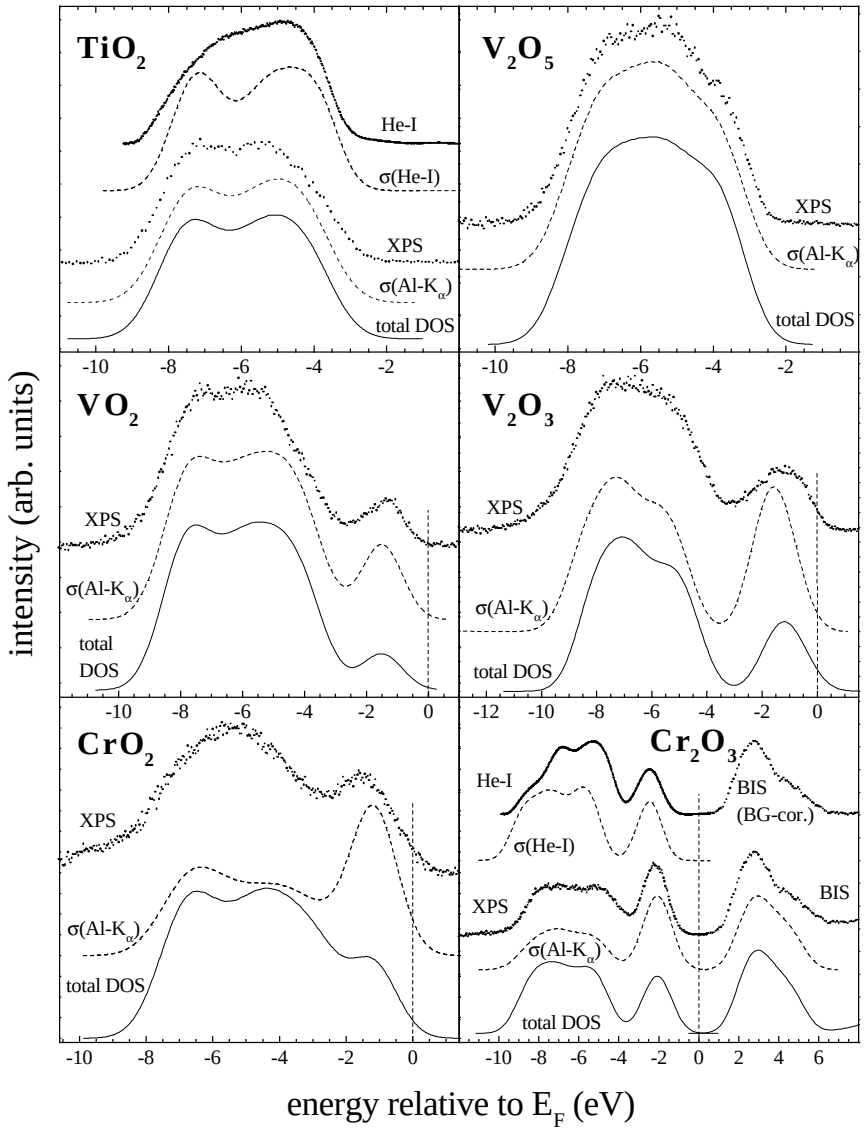

Figure 14. Comparison of measured photoemission and inverse photoemission (BIS) spectra (dots) with theoretical total (solid curves) and cross-section-weighted (dashed curves) densities of states for the early TM oxides TiO_2, V_2O_5, VO_2, V_2O_3, CrO_2, and Cr_2O_3. For details see the text. In contrast to the case for figures 12 and 13, the energies are here referred to the *experimental* Fermi level.

experimental structures (1.5 eV for XPS and BIS, except for Cu_2O (1.2 eV); 1.2 eV for UPS, except for TiO_2 (1.0 eV) and Cu_2O (0.7 eV)). The incorrect DFT band gaps were adjusted by shifting the occupied and unoccupied parts of the calculated DOS such that their spectral onsets agree with those of the corresponding PE and BIS spectra.

The comparison has been performed in two different ways. In the simplest case the (convoluted) total DOS is directly compared with the experiment. This procedure, however, neglects the different photoabsorption cross sections (σ) of the O 2p and TM 3d orbitals,

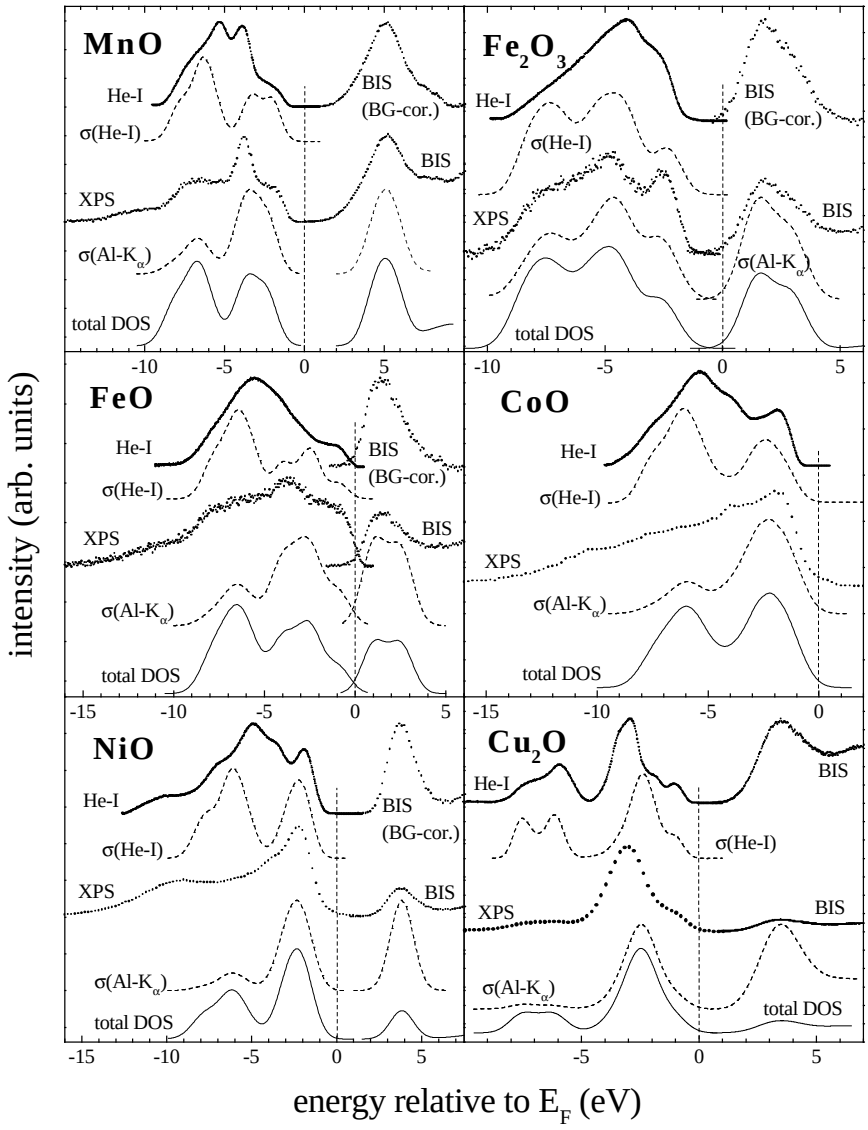

Figure 15. As figure 14, but for the late TM oxides MnO, Fe_2O_3, FeO, CoO, NiO, and Cu_2O.

which in addition depend on the photon energy [72]. Therefore, we have also calculated the cross-section-weighted sums of the corresponding partial densities of states for excitation with Al Kα and He I radiation. Other orbitals like the TM 4s states were neglected, because their PDOS and cross sections are small relative to those of O 2p and TM 3d.

In figures 14 and 15 the VB PE spectra are corrected for a Shirley-type background and matched in intensity to the same maximum height as the occupied part of the corresponding (total and σ-weighted) DOS. BIS spectra are presented in two ways:

(a) scaled such that for each oxide the intensity ratio between the XPS VB and BIS spectra matches that between the calculated occupied and unoccupied DOS; and

(b) corrected for a polynomial background (except for Cu_2O) and normalized (together with the σ(Al Kα)-weighted PDOS) to the same height as the occupied DOS in order to allow a better representation of their spectral shape.

We start the comparison of experimental and theoretical data with the early TMOs (figure 14). For TiO_2 and V_2O_5 the valence band spectra are fairly structureless and agree well with theory. The almost negligible difference between the total and cross-section-weighted (occupied) DOS in these compounds results from the fact that they are dominated by O 2p states, with the small occupied TM 3d weight uniformly distributed over the entire valence band range (cf. figure 12). For the following vanadium and chromium oxides, a new peak appears on the low-binding-energy side of the main valence band. Because its weight is correlated with the formal d occupation, it is tempting to attribute it to the increasing population of the 3d shell. As already discussed above for the vanadium oxides, the band calculations show that it does indeed have predominantly 3d character with non-negligible O 2p weight admixed with it. The measured spectra show good correspondence with the total DOS, whereas the σ-weighted DOS overemphasizes the '3d peak'. This could indicate that its 3d character, whose cross section dominates in the Al Kα spectra shown here, is actually smaller than calculated, implying an underestimation of O 2p–TM 3d hybridization. Another possibility is a systematic error in the calculated cross sections [72]. Good agreement is also found for the unoccupied states in Cr_2O_3, where it was possible to take a BIS spectrum.

Going on to the late TMOs (figure 15), the comparison between experiment and band-structure calculations becomes rather unsatisfactory. For MnO, FeO, CoO, and NiO, neither the total nor the partial DOS match the PE spectra satisfactorily. In all cases the calculated DOS displays an intensity dip at a binding energy of about 4 to 6 eV, which separates the 'O 2p' and 'TM 3d' parts of the valence band from each other. This dip is not observed experimentally. Only the intensity ratio between the low- and high-binding-energy range is roughly reproduced by the σ-weighted DOS. Reasonable agreement is, however, found for the BIS spectra, which according to band theory reflect transitions into unoccupied states of mostly TM 3d character. In contrast to those of the monoxides, the XPS spectra of Fe_2O_3 are reasonably well reproduced by the theoretical curves, especially by that based on the partial DOS. However, the agreement deteriorates with decreasing photon energy.

From this comparison, we thus find a trend of the band theory to become increasingly unreliable as one goes along the TM series. This correlates with the growing importance of on-site Coulomb repulsion, as we will discuss in the next section. A good band-structure description is only obtained for the early TMOs, particularly for those with a formal d^0 occupation [73]. However, it should be pointed out that the band picture cannot be complete, because it does not account for the PE satellites observed in the core spectra of *all* TM oxides. These result from electronic correlations outside the scope of the one-electron approach.

A notable exception from the failure of band theory for the late TMOs is the case of Cu_2O (see figure 15). Although the separation of the mainly Cu 3d-like and O 2p-like parts at 3 and 7 eV, respectively, comes out somewhat too large in the theory, the overall intensity distribution and spectral shape is fairly well reproduced by the σ-weighted DOS. Compared to that for the monoxides, the agreement is certainly much improved. This is presumably related to the fact that the Cu 3d shell is formally fully occupied, leaving no phase space for d–d correlations. The situation is thus equivalent to that of the d^0 systems. On the other hand, the band calculation predicts the existence of Cu 3d holes due to hybridization, which is confirmed by the BIS spectrum of Cu_2O. However, the hybridization does not seem to affect the closed-shell character of the electronic valence states, at least as far as correlations are concerned.

Finally, we note that the gap energies deduced from the combined XPS/BIS spectra are very close to the optical gaps published in the literature, if the XPS–BIS separation is measured from the inflection points of their respective onsets (see table 1).

6. Discussion

As already discussed above, DFT takes full account of the Coulomb correlation in the ground state, except for the approximations involved with the L(S)DA and GGA. The good correspondence between band theory and experimental excitation spectra for the early TMOs therefore suggests that additional correlation effects in the $(N-1)$ (PE) or $(N+1)$-electron (BIS) final states are not important. In other words, the extra hole or electron generated in these spectroscopies is screened out sufficiently well that the residual effects of the Coulomb interaction can be treated within an *effective* one-electron approach such as DFT. This is only possible if the charge carriers become mobile, i.e., if the local character of the 3d electrons stabilized by the on-site Coulomb repulsion is overcome by a pronounced TM 3d–O 2p hybridization (3d hopping between neighbouring TMs plays a minor role here, because the interatomic TM–TM distances are much larger than those between the TM and oxygen). The reduced strength of the final-state correlations in the early TMOs is reflected in the low (but still non-zero) intensities of the PE satellites relative to the main lines.

In contrast, final-state correlations are much stronger in the late TMOs. This can be best seen from the increasing intensity of the valence band satellite (at a binding energy of 10–12 eV; cf. figure 15) from MnO to NiO, which is partly responsible for the disagreement between the calculated DOS and the PE spectra. This indicates a more localized character of the 3d electrons in these compounds. We have already discussed the deviating behaviour of Cu_2O in terms of its formally closed 3d shell.

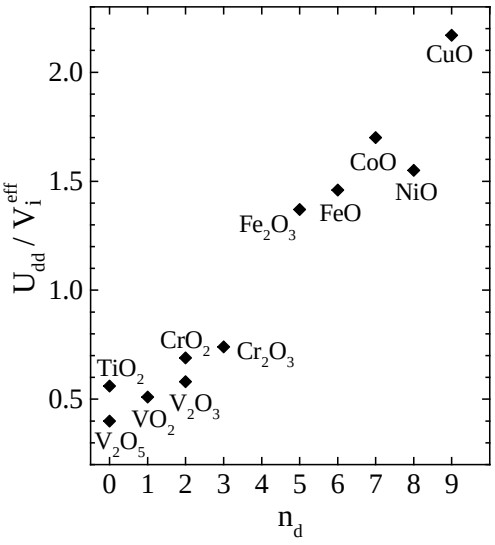

Figure 16. The ratio between the 3d correlation energy U_{dd} and the effective initial-state hybridization V_i^{eff} plotted versus the formal 3d occupation number n_d for a series of TM oxides (cf. table 2).

It is interesting to recast this interplay of Coulomb repulsion and covalency in the language of our cluster model. The electronic correlations are described here by the parameter U_{dd} which

stabilizes the ionic configuration. On the other hand, the hybridization between TM 3d and O 2p orbitals, entering the electronic structure through the parameter $V_i^{eff} = \sqrt{n_h} V_i$ (in the initial state), tends to delocalize the valence electrons, and thus reduces the effect of the on-site repulsion. Therefore, the ratio U_{dd}/V_i^{eff} can be viewed as an appropriate measure of the *effective* strength of interelectronic correlation and many-body effects in TM compounds. In figure 16 we plot the corresponding ratios for all TMOs studied with the present cluster model (cf. table 2) versus their respective formal TM 3d occupation n_d. One finds an almost linear trend from a reduced role of correlation effects ($U_{dd}/V_i^{eff} < 1$) in the early TMOs to their dominance (>1) in the late TMOs. As stated previously, this behaviour is mainly attributable to the decreasing number of holes n_h in going from TiO_2 to CuO, i.e. the smaller the phase space for oxygen-to-TM charge transfer becomes, the less effectively can the d–d Coulomb interaction be screened. The crossover from one regime to the other occurs between Cr_2O_3 and the following TMOs. This result supports the conclusions drawn from the comparison of the band calculations with the experimental spectra.

7. Conclusions

We have presented core-level and valence band photoemission and BIS spectra for a series of 3d-transition-metal oxides with formal TM 3d occupation n_d ranging from 0 to 10. The core-level spectra were interpreted in the framework of a simple cluster model based on the Anderson impurity model, yielding estimates for the parameters Δ, U_{dd}, and the effective hybridization V_i^{eff}. We observe a distinct increase of the relative correlation strength U_{dd}/V_i^{eff} from $\lesssim 0.5$ for the early TMOs to a value $\gtrsim 2$ for the late TMOs. This finding is consistent with the fact that for the former oxides the photoemission and inverse photoemission spectra of the valence states are rather well described by DFT band calculations. For the late TMOs the one-particle approach was found to fail due to strong many-body effects in the excited final states. The only exception is for Cu_2O, where the closed-shell character of the formal d^{10} configuration—being preserved upon hybridization—suppresses the phase space for d–d correlation. The strong hybridization in the early TMOs leads to a destabilization of an ionic ground state and to pronounced mixing of the configurations $|d^{n+q}\underline{L}^q\rangle$. As a consequence, the actual 3d ground-state occupation n_d^{cm} deviates significantly from the value n_d in the ionic limit. In particular, both the cluster model analysis and the density functional calculation yield, for the formally d^0 systems TiO_2 and V_2O_5, 3d occupations with $n_d^{cm} \gtrsim 1$. The crossover from the dominance of covalency to that of on-site Coulomb correlation occurs between Cr_2O_3 and Fe_2O_3.

There are several ways in which our many-body model could be improved to give a more detailed description of the electronic structure of these oxides. The literature contains a large number of such studies for individual TMOs. The goal of this work however was to obtain a gross picture of the electronic structure of the TMOs and derive general trends across the 3d-TM row by performing a systematic and internally consistent study of a complete series of oxides. For this purpose, our simple cluster model approach proved to capture the essential relevant physics. The result confirms previous studies on selected TMOs in that the original Mott–Hubbard description, in which U_{dd} is thought to be the single most important parameter, is inappropriate for these oxides: while the late TMOs can be characterized as charge-transfer insulators ($V^{eff} \approx V < \Delta < U_{dd}$), the electronic structure of the early TMOs is dominated by strong (effective) covalency ($V^{eff} \gg V \approx \Delta \approx U_{dd}$).

Acknowledgments

We wish to thank S Horn (Universität Augsburg) for providing the V_2O_5 single crystals, A Frantzen (Universität des Saarlandes) for the preparation of the VO_2 and V_2O_3 samples, C Ogglesby (Lucent Technologies) for additional V_2O_3 crystals, and D Reinen (Universität Marburg) for the CrO_2 powder. The authors are also obliged to A Kołodziejczyk (University of Mining and Metallurgy, Cracow, Poland) for supplying the iron oxide single crystals. We further acknowledge valuable discussions with A Kotani, T Uozumi, and H Ogasawara (University of Tokyo). This work was supported by the Deutsche Forschungsgemeinschaft (DFG), the Bundesministerium für Bildung und Forschung (BMBF), and by the European Union under Contract No CHRX-CT94-0502. PB was supported by the Austrian Science Foundation, Project No P10847.

References

[1] Mott N F 1949 *Proc. Phys. Soc.* A **62** 416
[2] Mott N F 1956 *Can. J. Phys.* **34** 1356
[3] Mott N F 1961 *Phil. Mag.* **6** 287
[4] Hubbard J 1963 *Proc. R. Soc.* A **276** 238
[5] Hubbard J 1964 *Proc. R. Soc.* A **277** 237
[6] Hubbard J 1964 *Proc. R. Soc.* A **281** 401
[7] Wilson J A 1972 *Adv. Phys.* **21** 143
[8] Wilson J A 1973 *Phase Transitions* ed L E Cross (New York: Pergamon) p 101
[9] Wilson J A 1985 *Metallic and Non-Metallic States of Matter* ed P P Edwards and C N R Rao (London: Taylor and Francis) p 215
[10] van der Laan G, Westra C, Haas C and Sawatzky G A 1981 *Phys. Rev.* B **23** 4369
[11] Kotani A and Toyozawa Y 1973 *J. Phys. Soc. Japan* **35** 1073
[12] Kotani A and Toyozawa Y 1973 *J. Phys. Soc. Japan* **35** 1082
[13] Kotani A and Toyozawa Y 1974 *J. Phys. Soc. Japan* **37** 912
[14] Anderson P W 1961 *Phys. Rev.* **124** 41
[15] Gunnarsson O and Schönhammer K 1983 *Phys. Rev.* B **28** 4315
[16] Gunnarsson O and Schönhammer K 1985 *Phys. Rev.* B **31** 4815
[17] Kotani A, Mizuta H, Jo T and Parlebas J C 1983 *Solid State Commun.* **53** 805
[18] Zaanen J, Westra C and Sawatzky G A 1986 *Phys. Rev.* B **33** 8060
[19] Asada S and Sugano S 1976 *J. Phys. Soc. Japan* **41** 1291
[20] Larsson S 1975 *Chem. Phys. Lett.* **32** 401
[21] Larsson S 1976 *Chem. Phys. Lett.* **40** 362
[22] Zaanen J, Sawatzky G A and Allen J W 1985 *Phys. Rev. Lett.* **55** 418
[23] Sawatzky G A and Allen J W 1984 *Phys. Rev. Lett.* **53** 2339
[24] Lee G and Oh S-J 1991 *Phys. Rev.* B **43** 14 674
[25] Okada K and Kotani A 1989 *J. Phys. Soc. Japan* **58** 2578
[26] Hüfner S 1994 *Adv. Phys.* **43** 183
[27] Parlebas J C 1992 *J. Physique* I **61** 1369
[28] Uozumi T, Okada K and Kotani A 1993 *J. Phys. Soc. Japan* **62** 2595
[29] Bocquet A E, Mizokawa T, Morikawa K, Fujimori A, Barman S R, Maiti K, Sarma D D, Tokura Y and Onoda M 1996 *Phys. Rev.* B **53** 1161
[30] Uozumi T, Okada K, Kotani A, Zimmermann R, Steiner P, Hüfner S, Tezuka Y and Shin S 1997 *J. Electron Spectrosc. Relat. Phenom.* **83** 9
[31] Hüfner S 1985 *Z. Phys.* B **61** 135
[32] Li X, Liu L and Henrich V E 1992 *Solid State Commun.* **84** 1103
[33] Carter S A, Rosenbaum T F, Metcalf P, Honig J M and Spalek J 1993 *Phys. Rev.* B **48** 16 841
[34] Kołodziejczyk A 1994 Private communication
[35] Zimmermann R, Steiner P and Hüfner S 1996 *J. Electron Spectrosc. Relat. Phenom.* **78** 49
[36] Brückner W, Oppermann H, Reichelt W, Terukow J I, Tschudnowski F A and Wolf E 1983 *Vanadiumoxide* (Berlin: Akademie)
[37] Schwarz K 1986 *J. Phys. F: Met. Phys.* **16** L211

[38] Chamberland B L 1977 *Crit. Rev. Solid State Mater. Sci.* **7** 1
[39] Zimmermann R, Claessen R, Reinert F, Steiner P and Hüfner S 1998 *J. Phys.: Condens. Matter* **10** 5697
[40] Slater J C 1960 *Quantum Theory of Atomic Structure* (New York: McGraw-Hill)
[41] Fujimori A and Minami F 1984 *Phys. Rev.* B **30** 957
[42] Okada K and Kotani A 1992 *J. Phys. Soc. Japan* **61** 4619
[43] Zimmermann R 1996 *PhD Thesis* Universität des Saarlandes, Germany
[44] Blaha P, Schwarz K and Luitz J 1997 *WIEN97* TU Wien
This is an improved and updated Unix version of the original copyrighted *WIEN* code, which was published by Blaha P, Schwarz K, Sorantin P and Trickey S B 1990 *Comput. Phys. Commun.* **59** 399
[45] Blöchl P, Jepsen O and Anderson O 1994 *Phys. Rev.* B **49** 16 223
[46] Dufek P, Blaha P and Schwarz K 1994 *Phys. Rev.* B **50** 7279
[47] Dufek P, Blaha P, Sliwko V and Schwarz K 1994 *Phys. Rev.* B **49** 10 170
[48] Terakura K, Oguchi T, Williams A R and Kübler J 1984 *Phys. Rev.* B **30** 4734
[49] Perdew J P, Chevary J A, Vosko S H, Jackson K A, Pederson M R, Singh D J and Fiolhais C 1992 *Phys. Rev.* B **46** 6671
[50] Perdew J P 1991 *Electronic Structure of Solids '91* ed P Ziesche and H Eschrig (Berlin: Akademie)
[51] Engel E and Vosko S H 1993 *Phys. Rev.* B **47** 13 164
[52] Blaha P, Dufek P, Sliwko V and Schwarz K 1996 *J. Magn. Magn. Mater.* **140–144** 173
[53] Shirley D A 1972 *Phys. Rev.* B **5** 4709
[54] Tougaard S and Sigmund P 1982 *Phys. Rev.* B **25** 4452
[55] Tougaard S 1990 *J. Electron Spectrosc. Relat. Phenom.* **52** 243
[56] Steiner P, Zimmermann R, Reinert F, Engel T and Hüfner S 1996 *Z. Phys.* B **99** 479
[57] McFeely F R, Kowalczyk S P, Ley L and Shirley D A 1972 *Phys. Lett.* A **49** 301
[58] Shirley D A 1975 *Phys. Scr.* **11** 117
[59] van Vleck J W 1934 *Phys. Rev.* **45** 405
[60] Kinsinger V, Zimmermann R, Hüfner S and Steiner P 1992 *Z. Phys.* B **89** 21
[61] Kinsinger V, Sander I, Steiner P, Zimmermann R and Hüfner S 1990 *Solid State Commun.* **73** 527
[62] van Acker J F, Stadnik Z M, Fuggle J C, Hoekstra H J W M, Buschow K H J and Stroink G 1988 *Phys. Rev.* B **37** 6827
[63] Zimmermann R, Steiner P, Claessen R, Reinert F and Hüfner S 1999 *J. Electron Spectrosc. Relat. Phenom.* at press
[64] Okada K, Kotani A, Kinsinger V, Zimmermann R and Hüfner S 1994 *J. Phys. Soc. Japan* **63** 2410
[65] Tanaka A and Jo T 1994 *J. Phys. Soc. Japan* **63** 2788
[66] Okada K and Kotani A 1991 *J. Phys. Soc. Japan* **60** 772
[67] Karlsson K, Gunnarsson O and Jepsen O 1992 *J. Phys.: Condens. Matter* **4** 895
[68] Karlsson K, Gunnarsson O and Jepsen O 1992 *J. Phys.: Condens. Matter* **4** 2801
[69] Karlsson K, Gunnarsson O and Jepsen O 1992 *Phys. Rev.* B **45** 7559
[70] van Veenendaal M A and Sawatzky G A 1993 *Phys. Rev. Lett.* **70** 2459
[71] van Veenendaal M A, Eskes H and Sawatzky G A 1993 *Phys. Rev.* B **47** 11 462
[72] Yeh J J and Lindau I 1985 *At. Data Nucl. Data Tables* **32** 1
[73] Eyert V and Höck K-H 1998 *Phys. Rev.* B **57** 12 727
[74] Chauvet O, Forro L, Kos I and Miljak M 1995 *Solid State Commun.* **93** 667
[75] Shin S, Suga S, Taniguchi M, Fujisawa M, Kanzaki H, Fujimori A, Daimon H, Ueda Y, Kosuge K and Kachi S 1990 *Phys. Rev.* B **41** 4993
[76] Shin S, Tezuka Y, Kinoshita T, Kakizaki A, Ishii T, Ueda Y, Jang W, Takei H, Chiba Y and Ishigame M 1992 *Phys. Rev.* B **46** 9224
[77] Chamberland B L 1967 *Mater. Res. Bull.* **2** 827
[78] Adler D and Brooks H 1967 *Phys. Rev.* **155** 826
[79] Anisimov V I, Zaanen J and Andersen O K 1991 *Phys. Rev.* B **44** 943
[80] Fujimori A, Saeki M, Kimizuka N, Taniguchi M and Suga S 1986 *Phys. Rev.* B **34** 7318
[81] Wei P and Qi Z Q 1994 *Phys. Rev.* B **49** 10 864
[82] Ghijsen J, Tjeng L H, van Elp J, Eskes H, Westerink J, Sawatzky G A, and Czyzyk M T 1988 *Phys. Rev.* B **38** 11 322
[83] Zimmermann R 1991 *Diplomarbeit* Universität des Saarlandes, Germany